

THE IRON UNRESOLVED TRANSITION ARRAY IN ACTIVE GALACTIC NUCLEI

HAGAI NETZER,¹

Received 2003 October 23; accepted 2003 November 27

ABSTRACT

The unresolved transition array (UTA) of iron M-shell ions is a prominent absorption feature in the X-ray spectrum of many active galactic nuclei (AGNs). Modeling photoionized plasmas in attempt to match the observed silicon and oxygen lines fail to predict the level of ionization of iron as inferred by this feature. It is suggested that the discrepancy is due to underestimation of the low-temperature dielectronic recombination rates for iron M-shell ions. Modified ionization balance calculations, based on new (guessed) atomic data, support this idea. The results are shown and compared to the global properties of several observed UTAs. Implications for AGN absorbing gas are discussed including an analysis of the ionization parameter distribution in such sources. The need for real calculations of such atomic data is stressed.

Subject headings: galaxies: active — galaxies: nuclei — atomic data — atomic processes — X-rays: galaxies

1. INTRODUCTION

Chandra and *XMM-Newton* spectroscopy of active galactic nuclei (AGNs) show a rich spectrum of X-ray absorption lines superimposed on a power-law continuum. Common features in such spectra are H-like and He-like lines of the astronomically abundant elements and inner-shell lines of silicon, sulphur, iron and other elements (e.g. Kaspi et al. 2002, Behar and Netzer 2002). Among these, the $n=2-3$ inner-shell transitions of Fe I-Fe XVI (so called iron M-shell ions) are particularly strong. They have been observed in IRAS 13349+2438 (Sako et al. 2001), NGC 3783 (Kaspi et al. 2001), NGC 5548 (Steenbrugge et al. 2003) and in other sources showing warm absorber (WA) features. The lines are hard to resolve spectroscopically and form a broad unresolved transition array (UTA) around 16–17Å. A detailed investigation of these transitions is given in Behar, Sako & Kahn (2001). These authors comment on the early UTA observations, compute synthetic absorption spectra and provide abbreviated set of atomic parameters for these lines.

The UTA feature has been discussed in a couple of recent papers analyzing the 900 ks *Chandra* spectrum of NGC 3783. Krongold et al. (2003) used the feature to argue for a very low ionization absorber in this source while Netzer et al. (2003, hereafter N03) noted a disagreement between the predicted and observed wavelength of the feature. The equivalent width (EW) and the central wavelength of the UTA are potentially important diagnostics of AGN absorbers and it is important to resolve the uncertainties in the calculation of the feature. This paper provides a new look at recently observed AGN spectra and suggests a major revision in iron dielectronic recombination (DR) rates that can resolve the UTA problem. §2 describes the available data and the old calculations. In §3 I present new calculations of the spectral distribution of the UTA based on ad hoc increases in the DR rates and §4 summarizes the more important new findings of this work.

2. UTA OBSERVATIONS AND OLD CALCULATIONS

The iron UTA feature has now been observed in the X-ray spectrum of at least six AGNs. The first detection and its implications are discussed in Sako et al. (2001). These authors analyzed the *XMM-Newton* RGS spectrum of

IRAS 13349+2348 and noted the strong absorption feature at 16–17Å. They also produced a detailed comparison with the widths and EWs of other strong absorption lines in the spectrum of this sources. The feature was observed in the first *Chandra* HETG spectrum of NGC 3783 (Kaspi et al. 2001) and confirmed, with better measurements, by the second, 900 ks spectrum of the source (Kaspi et al. 2002). It was also observed in the RGS spectrum of this source by Blustin et al. (2003) and by Behar et al. (2003). UTA features have been detected in the RGS spectrum of NGC 5548 by Steenbrugge et al. (2003) and in the RGS spectrum of Mkn 766 by Mason et al. (2003). More tentative identifications are mentioned by Pounds et al. (2001) who observed the X-ray spectrum of Mkn 509 and by Kaspi et al. (2003) who found the signature of the feature in the RGS spectrum of the quasar MR2251-178.

To illustrate the possible range of shapes and EWs of the observed UTAs, I show in Fig. 1 the 10–20Å spectrum of four AGNs with good S/N over this wavelength range (for information on the data used see the figure caption). Two of the spectra show very strong UTAs. These are the low-state spectrum of NGC 3783 (N03) and the spectrum of IRAS 13349+2348 (Sako et al. 2001). The third case is MCG-6-30-15. The RGS spectrum of this source contains very strong and broad features that were interpreted as either due to broad relativistic emission lines (Branduardi-Raymont et al. 2001; Sako et al., 2003) or due to a dusty WA (Lee et al. 2001). Regardless of the exact model, the spectrum shows a dip over the wavelength range where a strong UTA is detected in the spectrum of NGC 3783. This is very likely due to iron M-shell absorption although a full model is required to prove this case. The fourth case is the *Chandra* LETG spectrum (obtained from the *Chandra* archive) of NGC 5548 that also shows a shallow absorption feature over the same range. The main conclusions of this comparison are the great similarity in width and central wavelength of these UTAs and the large range in the EW of the feature.

A detailed theoretical study of the UTA is given in Behar et al. (2001). These authors identify the strongest lines in the feature as due to 2p-3d transitions in iron M-shell ions and provide new atomic calculations (wavelengths, A values and autoionization rates) to enable their computation. They also list abbreviated atomic data and show synthetic spectra for all the relevant ions (Fe I–Fe XVI). Their published data set

¹ School of Physics and Astronomy, Raymond and Beverly Sackler Faculty of Exact Sciences, Tel-Aviv University, Tel-Aviv 69978, Israel.

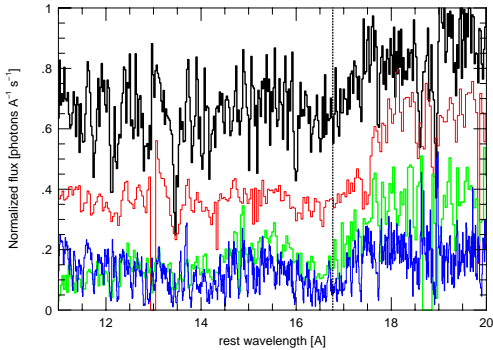


FIG. 1.— Normalized 10–20Å *Chandra* and *XMM-Newton* spectra of AGNs showing UTA features. From bottom to top: **NGC 3783** (data from N03). **IRAS13349+2438** (RGS data from the *XMM-Newton* archive, basically identical to the spectrum shown in Sako et al. 2001). **MCG-6-30-15** (259 ks RGS spectrum from the *XMM-Newton* archive). **NGC 5548** (339 ks LETG spectrum from the *Chandra* archive). The vertical line at 16.77Å marks the location of the O VII b-f edge.

includes mean wavelengths, summed f-values, summed lifetimes and total widths (in Å) of the main M-shell absorption features in all those ions. The paper contains several models of photoionized plasma computed with XSTAR (Kallman and Krolik 1995) and pertaining to AGN absorbers. They also comment on various other issues such as the total absorbing column deduced from the iron M-shell lines and the conditions for line saturation.

More recent calculations are provided by Krongold et al. (2003) and N03 who analyzed the 900 ks *Chandra* HETG spectrum of NGC 3783. Krongold et al. modeled the spectrum by two absorbers and used the observed wavelength of the UTA feature as their strongest evidence for a very low ionization parameter component. They also used the shape of the feature to argue against a flat ionization distribution of absorbers (see below). Their calculations are performed by G. Ferland’s photoionization code CLOUDY which was supplemented by an extensive list of atomic f-values for many elements and ions. The abbreviated Behar et al. (2001) atomic data set was used for calculation the UTA spectrum. N03 present a more complex absorber made of three ionization components and six kinematic components. The calculations are made with ION2003, the 2003 version of ION (Netzer 1996). This code contains the full atomic data set for the iron M-shell ions (provided by E. Behar) with many A-values and autoionization rates for each of the ions. N03 argue for a noticeable disagreement between the predicted and the observed level of ionization of iron, as inferred from the UTA measurements (see §3) and suggest that the reason may be the DR rates for the iron M-shell ions. The differences between the N03 and the K03 interpretations are much larger than expected from the differences in the atomic data used by the two groups. This putative discrepancy is discussed in the following sections.

3. NEW CALCULATIONS

This section suggest a way to cure the discrepancy between the observations and the calculations of the iron lines and provided new calculations to test this idea.

3.1. Low temperature dielectronic recombination rates for iron

Radiative recombination (RR) and DR rates for iron have been discussed extensively in the literature (see Arnaud and Raymond 1992, hereafter AR92; Mazzota et al., 1998; Savin et al. 2002; Savin et al. 2003; Gu 2003a, Gu 2003b). In short, there are reasonably accurate calculations of RR rates for almost all iron ions and a few laboratory measurements and theoretical calculations for $\Delta n = 1$ (so called “high temperature”) DR rates for iron L-shell ions. There are also some calculations of high-temperature DR rates for iron M-shell ions. The situation regarding $\Delta n = 0$ (“low temperature”) DR rates is more problematic. There are some estimates and several measurements for the L-shell ions but the rates for the M-shell ions are basically unknown and there are no laboratory measurements to identify and measure the relevant resonances. The only exception is the case of Fe XVI where several resonances have been measured and converted to DR rates (Linke-mann et al. 1995; Muller, 1999). Since low-temperature DR rates in other elements are comparable or even exceed the RR rates (Nussbaumer and Storey, 1983, 1984, 1986, 1987), this is likely to be the case for at least some iron ions (e.g. the above mention DR rates for Fe XVI are orders of magnitude larger than the Arnaud and Raymond (1992) theoretical rates). Thus the ionization balance of iron in photoionized plasmas where M-shell ions are the most abundant, is rather uncertain.

The older RR and DR rates for iron ions used in photoionization codes like CLOUDY and ION are mostly from the compilation of AR92. Extensive tests, over a large range of density and ionization parameter show that the new Gu (2003b) DR rates for the L-shell iron ions produce similar fractional ionizations to the AR92 rates (the seemingly large deviations illustrated in Gu 2003b, Fig. 22, are for much higher temperatures typical of collisional plasmas). Regarding the iron M-shell ions, the Arnaud and Raymond (1992) compilation give basically high temperature rates and the low-temperature recombination is controlled primarily by RR

As argued in N03, the new X-ray observations of NGC 3783 show a discrepancy between the ionization fraction of iron and various other elements. In particular, the level of ionization of iron deduced from the central wavelength and the shape of the UTA feature indicates lower ionization parameter compared with the one deduced from several oxygen and silicon lines. The best example is the comparison of the EWs of Si IX, Si X and Si XI lines, near 7Å with the EW and central wavelength of the iron UTA. According to N03, all those features originate in the lowest ionization component (the one with $\log(U_{OX}) = -2.4$ where U_{OX} is the “oxygen ionization parameter” defined over the 0.54–10 keV range). The above silicon lines are well separated and easy to measure in the spectrum of NGC 3783. Their f-values have recently been calculated by Behar and Netzer (2002) and other atomic data for silicon ions are reasonably well known. Thus, the column densities deduced from the measured EWs of those ions are reliable ionization parameter measures. For the deduced ionization parameter, Fe X–Fe XII are calculated to be the dominant iron ions. However, the UTA observation corresponds to Fe VIII–Fe X, i.e. a considerably more neutral iron. A similar discrepancy is found when comparing the oxygen level of ionization with that of iron while the oxygen and silicon levels of ionization seem to be consistent with each other. K03 also discussed the silicon-iron discrepancy and noted that their best model fails to predict the observed intensities of the Si X and

TABLE 1. PRESENT AND AR92 RR+DR RATES^a

Ion/ T_e	10^4 K	2×10^4 K	5×10^4 K	C_0
Fe VI	1.33	1.87	1.95	1.8×10^{-4}
Fe VII	1.32	1.86	2.09	2.7×10^{-4}
Fe VIII	1.31	1.85	2.09	3.8×10^{-4}
Fe IX	1.34	1.95	1.26	5.7×10^{-4}
Fe X	1.31	1.88	1.43	7.0×10^{-4}
Fe XI	1.30	1.85	2.14	8.2×10^{-4}
Fe XII	1.30	1.85	2.14	1.0×10^{-3}
Fe XIII	1.30	1.85	2.05	1.2×10^{-3}
Fe XIV	1.36	1.89	1.98	1.1×10^{-3}
Fe XV	1.34	1.85	1.61	1.2×10^{-3}

^aThe numbers in the table give the ratio of the present to the AR92 total recombination rates. Column 5 gives the additional constant for the new DR rate in equation 1.

Si XI lines.

The discrepancy in the level of ionization of the absorbing gas in NGC 3783 cannot be cured by changing the density, the spectral energy distribution (SED) or any other parameters of the model. (Note that high density suppression of DR rates must have an effect at some density which is probably well above the one deduced for NGC 3783. Obviously such atomic data are not yet available). Changing the iron abundance by factors of 3–5 does not help either. Lowering the ionization, as suggested by Krongold et al. (2003), improves the fit of the UTA wavelength but results in a poor fit of the silicon lines. I therefore suggest that the origin of the disagreement is the underestimation of the low temperature $\Delta n = 0$ DR rates for the iron M-shell ions. This assumption is investigated in the following section.

3.2. Assumed low-temperature DR rates

The standard expression for fitting DR rate coefficients is

$$\alpha_{DR} = T_e^{-3/2} \sum C_i \exp(-E_i/kT_e) \quad (1)$$

where C_i are fitting constants, E_i are energies expressed in temperature units and T_e the electron temperature. The procedure adopted here is to add a *single term* to the existing formula for each of the ions Fe VI–Fe XV with constants C_0 and E_0 , to represent a guess of the low temperature DR rate. The additional terms were chosen such that $E_0/k = 3 \times 10^4$ K and the new α_{DR} equals the RR rate at that temperature. This results in a small increase of the total rate at $T_e = 10^4$ K and an increase by factors of 2–3 at $2 \times 10^4 - 10^5$ K. The ratio of the new total (RR+DR) rates to the older values, at various representing temperatures, are given in Table 1. Also listed are the chosen values of C_0 for relevant iron ions.

The above prescription is only one out of several possible ways to artificially increase the low temperature DR rates. The only observational handle on such atomic rates is related to UTA observations and different choices of the values of E_0 and C_0 might work just as well. All prescriptions of this type result in a large increase (~ 3) of the total recombination rate at $T_e \simeq 10^5$ K. However, in photoionized gas, such temperatures are normally found in regions dominated by L-shell rather than M-shell iron ions. Thus the main effect of the new rates is on the ionization balance in those regions where the electron temperature is $1 - 4 \times 10^4$ K.

Several models of photoionized plasma have been computed to explore the effect of the new DR rates on the ioniza-

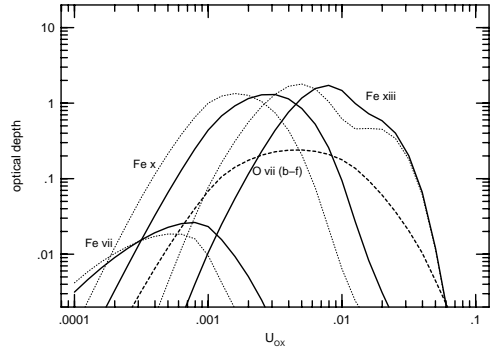


FIG. 2.— Optical depths of the leading (largest cross section) Fe VII, Fe X and Fe XIII lines and the O VII bound-free absorption edge as a function of the ionization parameter. Solid line: present DR rates. Dotted line: AR92 DR rates. Other model parameters are given in §3.2.

tion balance of iron. The method of calculation and all atomic data, except for the present DR rates, are similar to the ones discussed in N03. The assumed SED is the N03 NGC 3783 continuum with a 0.1–50 keV photon index of $\Gamma = 1.8$. The gas density is low (of order 10^5 cm⁻³ such that collisional excitation of high levels are negligible and the gas composition is the one given in N03 (Table 2). The chosen hydrogen column density is $10^{21.5}$ cm⁻² and the turbulent velocity 250 km s⁻¹. This combination was chosen to represent those cases that show clear iron absorption lines and O VII absorption edge. Saturation of the strongest iron lines can become important at such column densities. This was taken into account in the line excitation process but the calculated line profiles were assumed to be Gaussian.

Fig. 2 shows the optical depth of the leading lines (those with the largest absorption cross section) of several iron M-shell ions as a function of U_{OX} for the present and the AR92 DR rates. Also shown is the optical depth of O VII bound-free edge at 16.77Å. The use of the present rates has a significant influence on iron whose mean level of ionization is lowered by one or two ions for a given ionization parameter. The mean increase in $\log(U_{OX})$ required to obtain the level of ionization of iron obtained with the AR92 rates is about 0.2.

The present DR rates were also used to re-compute a full model for NGC 3783 using the six absorption components and the three emission components described in N03. Fig. 3 shows a comparison of the old and the new models with the low-state spectrum of the source (N03 Fig. 7). The diagram shows that the increased DR rates cause a significant shift in iron ionization and a much improved fit to the data. The level of ionization of iron, oxygen and silicon are now all consistent and the present rates seem to cure the ionization discrepancy (the silicon line fit over the 4–7Å band has not changed and is basically identical to the one shown in N03). Applications to the spectrum of other sources are more difficult to illustrate since we do not have satisfactory models for these cases.

3.3. Discrete versus continuous distribution of ionization

The Behar et al. (2001) work demonstrates the usefulness of the UTA observations in determining the level of ionization of the X-ray absorbing gas. In particular, the central wavelength of the feature is an indicator of the dominant iron

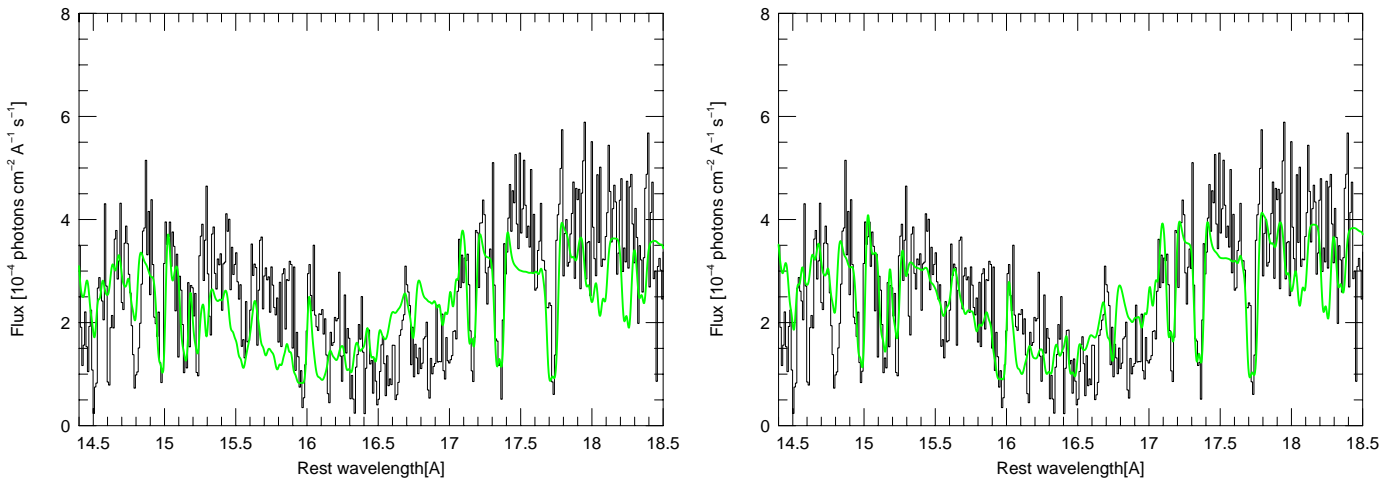


FIG. 3.— Left: Old fit to the low-state spectrum of NGC 3783 (from N03 Fig. 7). Right: Same model components but using the new DR rates.

ions. Thus, accurate UTA measurements can be used to test the idea, raised by Kinkhabwala et al. (2002) who studied the spectrum of the type II Seyfert NGC 1068, that the highly ionized emitting gas in AGNs indicates a flat distribution of ionization rather than a few discrete components. If type-I AGN absorbers are similar in their properties to type-II AGN emitters, this would mean that in such absorbers, many ions of the same element have comparable column densities. Such an ionization structure can be formed either due to a strong dependence of the ionization parameter on the distance from the center or due to multi-component multi-density medium at a given location (which is more likely to be the case for NGC 1068). A similar idea, by Krolik and Kriss (2001), involves a medium with a smooth distribution of temperatures and ionization parameters. The predicted spectroscopic differences are clear. A single ionization component will result in a relatively narrow UTA while the suggested flat distribution will produce a much broader feature.

The idea of a flat ionization distribution was further investigated by Krongold et al. (2003). These authors provided several calculations similar to those shown by Behar et al. (2001) to support the idea of a broader UTA for larger ionization parameter gas. They also argued that the sharply defined and relatively narrow UTA observed in the spectrum of NGC 3783 is inconsistent with the Krolik and Kriss (2001) suggestion since any mixture of ionizations will result in a broader and shallower feature.

To further test this suggestion, I calculated several multi-components photoionization models and compared them with “single shell” models. The calculations employ the new DR rates for the iron M-shell ions. One example, shown in Fig. 4 compares the combined spectrum of four absorbing shells spanning a large range of ionizations (a factor of $10^{1.5}$ in U_{OX}) with the spectrum of a single shell whose column density equals the sum of the four columns. The column density of each shell was 10^{21} cm^{-2} and the four ionization parameters were chosen such that in one shell O V is the most abundant oxygen ion, in the second O VI is most abundant, O VII dominates the third shell ionization and O VIII the fourth. The

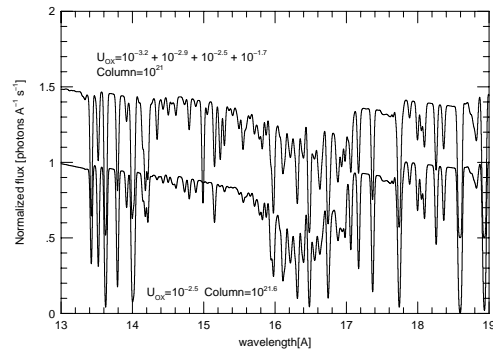


FIG. 4.— A comparison of a four component model with ionization parameters and column densities as marked (top curve) with a single component model with a column density of the total four columns and a “mean” ionization parameter (bottom curve). The wavelength covered by the UTA under such conditions is roughly 15.2–17.4Å. The column density and ionization parameter of the four components are marked at the top and those for the single shell at the bottom of the diagram. Note the great similarity in total width and central feature of the calculated UTAs.

total column densities of those ions, in all four shells, are: $10^{17.54} \text{ cm}^{-2}$ for O V, $10^{17.56} \text{ cm}^{-2}$ for O VI, $10^{17.80} \text{ cm}^{-2}$ for O VII, and $10^{17.52} \text{ cm}^{-2}$ for O VIII (note that it is difficult to obtain a more uniform distribution because several oxygen ions are present in each shell). The single-shell model column density is $10^{21.6} \text{ cm}^{-2}$ (identical to the column density of the low ionization component of Krongold et al. 2003), and $\log(U_{OX}) = -2.5$, roughly the mean of the four ionization parameters and similar to the lowest ionization parameter component in NGC 3783.

As shown in Fig. 4, the composite four shell spectrum and the single-shell spectrum produce very similar UTAs. The reason is that the thick single shell contains a mixture of oxygen ions which is not too different from the four-shell mixture. This is also true for the M-shell iron ions whose total column

densities in the four-component are comparable to the column densities in the single shell. In fact, the only significant difference between the two is the presence of a strong Fe XVII absorption line, near 15Å, in the four-component model. This is caused by the larger column density of high ionization iron in the four component spectrum.

The above result is very general and other combinations of somewhat smaller or larger column density shells lead to similar conclusions. In general, thicker shells contain broader distribution of ionizations and produce broader UTAs. As noted by Behar et al. (2001), and Krongold et al. (2003), higher mean ionization also result in broader UTAs yet all those single-shell cases can be broken into several sub components with a similar combined spectrum. Thus, UTA observations by themselves cannot be used to rule out the possibility of a multi-component, flat ionization parameter distribution of absorbers spanning 1–2 orders of magnitude in ionization parameter. This does not seem to be a consequence of the new DR rates since adding those rates result in roughly a constant shift of all ionization fractions as a function of U_{OX} (Fig. 2).

4. CONCLUSIONS

Detailed analysis and modeling of iron UTA features in AGN spectra suggest that the iron level of ionization is in-

consistent with the ionization of other elements. It is suggested that the reasons are the inaccurate DR rates used for the iron M-shell ions and new "assumed" rates are used to support this claim. Theoretical spectra using the new atomic data give much better fit to the observed spectrum of NGC 3783. It is also shown that UTA observations by themselves cannot be used to distinguish between multi-component and single component low ionization AGN absorbers. New measurements and calculations of DR rates for M-shell lines are badly needed to produce more realistic models to the X-ray spectrum of AGN.

I am grateful to Daniel Savin and Ehud Behar for interesting and useful discussions. I also thank the referee, D. Liedahl, for his many useful suggestions. Shai Kaspi provided his great expertise in reducing the *Chandra* and *XMM-Newton* archival spectra. This work is supported by the Israel Science Foundation grants 545/00 and 232/03. I thank the astrophysics group at Columbia university for their hospitality during a summer visit in 2003.

REFERENCES

- Arnaud, M., & Raymond, J., 1992, ApJ, 398, 394 (AR92)
 Behar, E., & Netzer, H. 2002, ApJ, 570, 165
 Behar, E., Sako, M., & Kahn, S. M. 2001, ApJ, 563, 497
 Behar et al., 2003 (astro-ph/0307467)
 Blustin, A. J., Branduardi-Raymont, G., Behar, E., Kaastra, J. S., Kahn, S. M., Page, M. J., Sako, M., & Steenbrugge, K. C. 2002, A&A, 392, 453
 Branduardi-Raymont, G., Sako, M., Kahn, S. M., Brinkman, A. C., Kaastra, J. S., & Page, M. J. 2001, A&A, 365, L140
 Gu, M. F. 2003a, ApJ, 589, 1085
 Gu, M. F. 2003b, ApJ, 590, 1131
 Kallman, T.R., & Krolik, J.H., 1995, XSTAR, a spectral analysis tool (Greenbelt: NASA/GSFC HEASARC)
 Kaspi, S., et al. 2002, ApJ, 574, 643
 Kinkhabwala, A. et al. 2002, ApJ, 575, 732
 Krolik, J.H., & Kriss, G.A., 2001, ApJ, 561, 684
 Krongold, Y., Nicastro, F., Brickhouse, N.S., Elvis, M., Liedahl, D.A., & Mathur, S., 2003, ApJ preprint doi:10.1086/378639
 Lee, J. C., Ogle, P. M., Canizares, C. R., Marshall, H. L., Schulz, N. S., Morales, R., Fabian, A. C., & Iwasawa, K. 2001, ApJ, 554, L13
 Linkemann, J., et al. 1995, "Nuclear Instruments and Methods in Physics Research" Section B, v. 98, p. 154
 Mason, K. O. et al. 2003, ApJ, 582, 95
 Mazzotta, P., Mazzitelli, G., Colafrancesco, S., & Vittorio, N. 1998, A&AS, 133, 403
 Muller, A., 1999, Int. J. Mass Spectrom., 192, 9
 Netzer, H. 1996, ApJ, 473, 781
 Netzer, H., Chelouche, D., George, I. M., Turner, T. J., Crenshaw, D. M., Kraemer, S. B., & Nandra, ApJ, (in press), astro-ph-0309096 (N03)
 Nussbaumer, H., & Storey, P.J., 1983, A&A, 126, 75
 Nussbaumer, H., & Storey, P.J., 1984, A&AS, 56, 293
 Nussbaumer, H., & Storey, P.J., 1986, A&AS, 64, 545
 Nussbaumer, H., & Storey, P.J., 1986, A&AS, 69, 123
 Pounds, K., Reeves, J., O'Brien, P., Page, K., Turner, M & Nayakshin, S., 2001, ApJ, 559, 181
 Sako, M., et al., 2001, A&A 365, L168
 Sako, M., et al., 2003, ApJ, 596, 114
 Savin, D. W. et al. 2002, ApJ, 576, 1098
 Savin, D. W. et al. 2003, ApJS, 147, 421
 Steenbrugge, K.C. Kaastra, J.S., de Vries, C.P., & Edelson, R., 2003, A&A, 402, 477